

# Dalton Transactions

Accepted Manuscript



This is an *Accepted Manuscript*, which has been through the Royal Society of Chemistry peer review process and has been accepted for publication.

*Accepted Manuscripts* are published online shortly after acceptance, before technical editing, formatting and proof reading. Using this free service, authors can make their results available to the community, in citable form, before we publish the edited article. We will replace this *Accepted Manuscript* with the edited and formatted *Advance Article* as soon as it is available.

You can find more information about *Accepted Manuscripts* in the [Information for Authors](#).

Please note that technical editing may introduce minor changes to the text and/or graphics, which may alter content. The journal's standard [Terms & Conditions](#) and the [Ethical guidelines](#) still apply. In no event shall the Royal Society of Chemistry be held responsible for any errors or omissions in this *Accepted Manuscript* or any consequences arising from the use of any information it contains.

**Evidence of Cationic Mixing and Ordering in the Honeycomb Layer of  $\text{Li}_4\text{MSbO}_6$** **(M(III) = Cr, Mn, Al, Ga) (S.G.  $C2/c$ ) Oxides**

Neha Bhardwaj, Akanksha Gupta and S. Uma\*

Materials Chemistry Group, Department of Chemistry,

University of Delhi, Delhi 110 007, INDIA

**Abstract**

We report the synthesis of the rock salt derived structures of  $\text{Li}_4\text{MSbO}_6$  (M (III) = Cr, Mn, Al, Ga) oxides. These layered oxides in addition to the cation- ( $\text{Li}^+$  ions versus ( $\text{Li}^+/\text{M}^{3+}/\text{Sb}^{5+}$ ) ions) ordering as observed in several  $\alpha\text{-NaFeO}_2$  type oxides, are shown to have the formation of preferred cationic mixing in the  $(\text{LiMSbO}_6)^{3-}$  layers based on single crystal and powder XRD studies. The additional ordering found in the honeycomb layer is justified by the oxygen octahedra formed by more Sb/less Li, more Li/less M and more M/less Li/less Sb. This preferential cation mixing is proven structurally for the first time in these oxides and is evident from the superstructure observed by the doubling of the  $c$  axis ( $C2/c$ :  $a \approx 5.11$ ;  $b \approx 8.85$ ;  $c \approx 9.84$  Å;  $\beta \approx 100^\circ$ ) as compared to  $\text{Li}_4\text{FeSbO}_6$  ( $C2/m$ :  $a = 5.165(6)$ ;  $b = 8.928(13)$ ;  $c = 5.155(7)$  Å;  $\beta = 109.47(2)^\circ$ ). The driving force seems to be the minimization of various cation-cation ( $\text{Sb}^{5+}\text{-Sb}^{5+}$ ,  $\text{Sb}^{5+}\text{-M}^{3+}$ ,  $\text{M}^{3+}\text{-M}^{3+}$ ) interactions expected in the edge shared octahedral structures. The magnetic susceptibility of the oxides with magnetic metal ions in triangular lattice follows Curie-Weiss law in the temperature range (300K - 75K) for  $\text{Li}_4\text{CrSbO}_6$  and in the temperature range (300K - 50K) for  $\text{Li}_4\text{MnSbO}_6$  with negative values of Weiss constants at 67 K and 68 K respectively. At low temperatures (< 7K) antiferromagnetic interactions are expected because of the interaction between the layers. Ionic conductivity measurements of  $\text{Li}_4\text{MSbO}_6$  and ion-exchange experiments with  $\text{Ag}^+$  ions resulting in delafossite based oxides confirmed the mobility of interlayer lithium ions in these oxides.

---

**\*Corresponding Author****E-mail: [suma@chemistry.du.ac.in](mailto:suma@chemistry.du.ac.in)**

## 1. Introduction

The well-known cathode material,  $\text{LiCoO}_2$ <sup>1</sup> along with other battery and thermoelectric material  $\text{Na}_x\text{CoO}_2$ <sup>2, 3</sup> belong to the  $\text{AMO}_2$  type oxides having octahedral brucite layers formed by transition metal (M) ions that are separated by alkali metal ions. These  $\text{AMO}_2$  structural type is gaining momentum because of the possibility of several combinations of metal ions with various oxidation states that are possible at the M site,<sup>4</sup> resembling other popular structural families such as the perovskites and pyrochlores existing in the field of solid state chemistry (Table S1). As far the substitution of metal ions, the finding of  $\text{O3-Na}_2\text{Cu}_2\text{TeO}_6$ <sup>5</sup> followed by the reports of a series of fast ion conductors,  $\text{P2-Na}_2\text{M}_2\text{TeO}_6$  (M = Ni, Zn, Mg)<sup>6, 7</sup> opened up many interesting possibilities.  $\text{Li}_3\text{M}_2\text{XO}_6$  and  $\text{Na}_3\text{M}_2\text{XO}_6$  (M = Mg, Co, Ni, Cu, Zn; X = Nb, Ta, Sb, Bi)<sup>8-16</sup> are examples with a different A to M ratio from the previous tellurium series and discovered over the past decade with some of them in the recent past.

These ordered rocksalt oxides possess layered structures in such a way that divalent or trivalent magnetic or non magnetic M ions together with pentavalent X (Nb, Ta, Sb, Bi) ions may form the honeycomb layers separated by non magnetic alkali metal oxygen octahedral layers. In the case of honeycomb layers formed by magnetic ions because of magnetic frustration, interesting magnetic properties such as antiferromagnetic ordering and spin gap behavior arise. Such phenomena are reported for M =  $\text{Co}^{2+}$  (e.g.  $\text{Na}_3\text{Co}_2\text{SbO}_6$ , and  $\text{Na}_2\text{Co}_2\text{TeO}_6$ ), for M =  $\text{Ni}^{2+}$  (e.g.  $\text{Li}_3\text{Ni}_2\text{SbO}_6$ ) and for M =  $\text{Cu}^{2+}$  (e.g.  $\text{Na}_3\text{Cu}_2\text{SbO}_6$ ,  $\text{Na}_2\text{Cu}_2\text{TeO}_6$ ) containing oxides. We reported<sup>17, 18</sup> recently  $\text{Li}_8\text{M}_2\text{Te}_2\text{O}_{12}$  and  $\text{Li}_8\text{M}_2\text{Sb}_2\text{O}_{12}$  oxides referred hence forth uniformly as  $\text{Li}_4\text{MTeO}_6$  (M(II) = Co, Ni, Cu, Zn) and  $\text{Li}_4\text{MSbO}_6$  (M(III) = Cr, Fe, Al, Ga) series of oxides, wherein the structures

for  $\text{Li}_4\text{CoTeO}_6$ ,  $\text{Li}_4\text{CuTeO}_6$  and  $\text{Li}_{3.90}\text{Cu}_{1.33}\text{Te}_{0.94}\text{O}_6$  were solved by single crystal X-ray diffraction for the first time, and were accompanied by the independent study of  $\text{Li}_4\text{ZnTeO}_6$ <sup>19</sup> and  $\text{Li}_4\text{FeSbO}_6$ .<sup>20</sup> The occurrence of  $\text{Cu}^{2+}$  ions in varying amounts were found with the interlayer  $\text{Li}^+$  ions, leading to interesting magnetization behavior even at room temperature.<sup>17</sup> Our results included another Li-Cu-Te-O oxide,  $\text{Li}_2\text{Cu}_2\text{TeO}_6$ , isostructural with  $\text{Na}_2\text{Cu}_2\text{TeO}_6$  attained only by low temperature lithium ion-exchange along with two structural polymorphs of  $\text{Li}_2\text{Ni}_2\text{TeO}_6$ .<sup>18</sup> The importance of investigating these oxides have shown to be particularly useful by the subsequent report<sup>21</sup> of  $\text{Li}_4\text{NiTeO}_6$  as a potential cathode material for Li-ion batteries.  $\text{Li}_4\text{FeSbO}_6$  itself was found to show antiferromagnetic ordering ( $T_N \approx 3.6\text{K}$ ) and was characterized by a variety of measurements including powder X-ray diffraction, cyclic voltametry, magnetic susceptibility and heat capacity etc.<sup>20</sup> Since our earlier report contained only the preliminary results on the formation of  $\text{Li}_4\text{MSbO}_6$  ( $\text{M(III)} = \text{Cr, Fe, Al, Ga}$ ), a detailed structural and physical characterization of  $\text{Li}_4\text{MSbO}_6$  ( $\text{M(III)} = \text{Cr, Fe, Al, Ga}$ ) oxides have been carried out and interestingly the series could be expanded by synthesizing  $\text{Li}_4\text{MnSbO}_6$  containing another magnetic  $\text{Mn(III)}$  ions. In the case of  $\text{Li}_4\text{CrSbO}_6$ , the structure has been determined by both single crystal as well as by powder X-ray diffraction method, while Reitveld refinements of powder X-ray diffraction patterns confirmed the structure of other  $\text{Li}_4\text{MSbO}_6$  ( $\text{M(III)} = \text{Mn, Ga}$ ) members. The oxides  $\text{Li}_4\text{MSbO}_6$  ( $\text{M(III)} = \text{Cr, Mn, Al, Ga}$ ) crystallizing in space group  $C2/c$  differ from  $\text{Li}_4\text{FeSbO}_6$  (S.G.  $C2/m$ ) in the manner in which the ions ( $\text{Li}^+$ ,  $\text{M}^{3+}$  and  $\text{Sb}^{5+}$ ) were distributed to form the honeycomb  $(\text{LiMSbO}_6)^{3-}$  layers. The results from structural investigations revealed that while a perfect  $(\text{LiO}_6)/(\text{M}^{\text{III}}\text{O}_6)/(\text{SbO}_6)$  ordering was missing,

preferred cationic mixing of ( $\text{Sb}^{5+}/\text{Li}^+$ ), ( $\text{Li}^+/\text{M}^{3+}$ ), ( $\text{M}^{3+}/\text{Li}^+/\text{Sb}^{5+}$ ) was sufficient to show a different superstructure in these oxides. The results are discussed in detail in this article.

## 2. Experimental Section

### 2.1. Synthesis

Conventional ceramic methods were adopted to prepare the oxides with the stoichiometry  $\text{Li}_4\text{MSbO}_6$  ( $\text{M(III)} = \text{Cr, Mn, Fe, Al, Ga}$ ). The reactants used were all of Sigma Aldrich with purity of  $\geq 99\%$ . Stoichiometric amounts of the reactants such as  $\text{Li}_2\text{CO}_3$ ,  $\text{Sb}_2\text{O}_3$ ,  $\text{Cr}_2\text{O}_3$ ,  $\text{MnO}$ ,  $\text{Fe}_2\text{O}_3$ ,  $\text{Al}_2\text{O}_3$ , and  $\text{Ga}_2\text{O}_3$  were thoroughly mixed, heated initially at  $650^\circ\text{C}$  for 12 h, and by finally heating at  $850^\circ\text{C}$  for 24h-48h with intermediate grindings. Single crystals of  $\text{Li}_4\text{CrSbO}_6$  were grown from the phase pure polycrystalline sample by increasing the temperature to  $1100^\circ\text{C}$  in a platinum crucible, followed by slow cooling ( $3^\circ\text{C/h}$ ) to  $950^\circ\text{C}$ , and then to  $850^\circ\text{C}$  at the rate of  $5^\circ\text{C/h}$  and was finally annealed to room temperature. Crystals were green in colour and used for single crystal X-ray diffraction measurements. A phase pure  $\text{Li}_4\text{MnSbO}_6$  was obtained after heating at  $1000^\circ\text{C}$  for 12-24 h. Ceramic samples for AC conductivity measurement were carried out for hard pressed calcined powder samples in pellets form, which were then heated again at  $850^\circ\text{C}$ . They were polished with silver paste, dried, and then utilized for impedance spectroscopy measurements. Ion exchange reactions were also carried out at  $250^\circ\text{C}$  for 1 h by mixing the parent lithium oxide with  $\text{AgNO}_3$  in the 1:3 ratio. After the reaction, the products were washed with distilled  $\text{H}_2\text{O}$  and dried at  $\sim 60^\circ\text{C}$ .

### 2.2. Characterization

The powder X-ray diffraction (PXRD) patterns were collected using high resolution PANalytical diffractometer, equipped with pixel detector employing  $\text{Cu K}_\alpha$  radiation ( $\lambda$

= 1.5418 Å) obtained with a scan rate of 92.82 s/step and step size 0.013° at 298 K. The PXRD patterns were fit using the LeBail method to obtain the cell dimensions and Reitveld refinement of the PXRD patterns were carried out using GSAS+EXPGUI program.<sup>22</sup> Single crystal XRD (SCXRD) data was recorded on an Oxford Xcalibur NOVA diffractometer with a four circle  $\kappa$  goniometer employing a graphite-monochromatized Mo  $K_{\alpha}$  ( $\lambda = 0.71073$  Å) radiation at room temperature. The diffraction intensities were corrected for Lorentz polarization effects and for absorption by multiple scan methods. The data were reduced using CrysAlisRED (special programs available with the diffractometer). The structure was solved by direct methods and refined using SHELXS 97<sup>23</sup> incorporated in WINGX suite.<sup>24</sup> AC conductivity measurements were performed on sintered (at 900 °C) pellets with a diameter of 1.3 cm in the frequency range 1 Hz to 10<sup>7</sup> Hz (Alpha N analyzer Novocontrol, Pt electrode). The magnetic measurements were carried out using a Quantum Design MPMS SQUID magnetometer under an applied field of 1T in the temperature range of 4-300 K. UV–VIS diffuse reflectance data were collected over the spectral range 200–1000 nm using Perkin-Elmer Lambda 35 scanning double beam spectrometer equipped with a 50 mm integrating sphere. BaSO<sub>4</sub> was used as a reference. The data were transformed into absorbance with the Kubelka–Munk function for the estimation of the band gap. The photoluminescence (PL) measurements were executed using Horiba Jobin Yvon Fluoro log-3 modular spectrofluorometer at room temperature employing CW xenon lamp source.

### 3. Results and Discussions

#### 3.1. Crystal Structures

The PXRD pattern of  $\text{Li}_4\text{FeSbO}_6$  (Fig. 1a) synthesized in the present study was in agreement very well to those reported earlier<sup>17, 20</sup> and the refined lattice parameters in a S.G.  $C2/m$  are  $a = 5.198(7) \text{ \AA}$ ;  $b = 8.994(4) \text{ \AA}$ ;  $c = 5.193(7) \text{ \AA}$ ;  $\beta = 99.9(1)^\circ$ . This structure type in  $C2/m$  symmetry was explained by the formation of  $(\text{LiFeSbO}_6)^{3-}$  honeycomb layer alternating with lithium layers.<sup>20</sup> The Reitveld refinement of the PXRD pattern resulted in a structure with mixing of  $\text{Sb}^{5+}$ - $\text{Fe}^{3+}$  and  $\text{Li}^+/\text{Fe}^{3+}/\text{Sb}^{5+}$  on the  $\text{Sb}^{5+}$  and  $\text{Zn}^{2+}$  positions of a structurally related compound such as  $\text{Li}_3\text{Zn}_2\text{SbO}_6$ .<sup>8</sup> The disordered nature of the layer stacking was evident from the sloping background in the  $2\theta$  range of  $19\text{-}25^\circ$ . However a careful examination of the PXRD patterns for the remaining M(III) ions namely Cr, Mn, Al, Ga (Fig. 1b-e) showed additional reflections that could not be indexed by a  $C2/m$  space group. The exclusion of possible  $C2/m$  superstructure automatically excludes the subcell  $R\bar{3}m$  ( $a \approx 2.9$ ;  $c \approx 14.5 \text{ \AA}$ ) structure and the metrically equivalent  $P3_1I2$  ( $a \approx 5.1$ ;  $c \approx 14.5 \text{ \AA}$ ) superstructure<sup>14</sup> (Fig. S1). The additional reflections (Fig. 1b-e) in the  $2\theta$  range ( $19\text{-}40^\circ$ ) could be accounted by doubling the  $c$  parameter of  $C2/m$  lattice dimensions and indexing using a S.G.  $C2/c$  ( $a \approx 5.11$ ;  $b \approx 8.85$ ;  $c \approx 9.84 \text{ \AA}$ ;  $\beta \approx 100^\circ$ ) structure (Tables S2-S6). A similar ordering has been known to occur in  $\text{Li}_2\text{MnO}_3$  ( $\text{Li}_3\text{LiMn}_2\text{O}_6$ )<sup>25</sup> and  $\text{Li}_2\text{TiO}_3$  ( $\text{Li}_3\text{LiTi}_2\text{O}_6$ )<sup>26</sup> oxides and in the recently reported<sup>27</sup>  $\text{Li}_3\text{Ni}_2\text{RuO}_6$ , wherein the honeycomb layer is made up of only two types of ( $\text{Li}^+/\text{Mn}^{4+}$ ,  $\text{Li}^+/\text{Ti}^{4+}$ ,  $\text{Ni}^{2+}/\text{Ru}^{4+}$ ) cations. Although the structure of  $\text{Li}_3\text{Cu}_2\text{SbO}_6$  was earlier described in  $C2/c$ ,<sup>11</sup> it was later shown to be  $C2/m$  based on the PXRD patterns.<sup>19</sup> Very recently Schmidt and coworkers reported O3- $\text{Na}_3\text{LiFeSbO}_6$  in the space group  $C2/c$  based on PXRD patterns and suggested the honeycomb formation by the ordering of  $\text{Li}^+$ ,  $\text{Fe}^{3+}$ ,  $\text{Sb}^{5+}$  ions.<sup>28</sup>

For the present  $\text{Li}_4\text{MSbO}_6$  ( $M = \text{Cr}, \text{Mn}, \text{Al}, \text{Ga}$ ) oxides the single crystal growth was further attempted to confirm the results arising out of the PXRD data. Single crystals were successfully obtained in the case of  $\text{Li}_4\text{CrSbO}_6$  and the lattice parameters confirmed a monoclinic symmetry. The systematic absences once again indicated a C-centred lattice with the possibility of  $C2/c$  space group. The positions supposedly occupied by the heavy atoms (Sb and Cr) were first located by direct methods. The O and the Li atoms were added from the difference Fourier map. The refinement consisted of Li1, Li2, O1, O2 and O3 atoms respectively in  $8f$ ,  $4d$ , and three  $8f$  positions (Table 1). Solving the structure in the  $C2/c$  space group has the possibility of resulting in a perfectly ordered cationic ( $\text{Li}^+$ ,  $\text{Cr}^{3+}$  and  $\text{Sb}^{5+}$ ) honeycomb octahedral layers unlike the  $C2/m$  space group, having only two available crystallographic sites for placing the three cations. Such an ordering may only exist when there is sufficient difference in the size and charge of these cations. However, considering the similar sizes of  $\text{Cr}^{3+}$  ( $\text{VI} = 0.615\text{\AA}$ ) and  $\text{Sb}^{5+}$  ( $\text{VI} = 0.60\text{\AA}$ ) versus the larger  $\text{Li}^+$  ( $\text{VI} = 0.76\text{\AA}$ ) ion, probability of their mixed occupancies are greater. The structural model consisting of a perfectly ordered arrangement of these ions resulted in a  $R_I$  factor around 22.2% and with a difference peak of  $38.5\text{\AA}^{-3}$ . The thermal parameters at this stage also suggested a mixed occupancy of  $\text{Li}^+$ ,  $\text{Cr}^{3+}$  and  $\text{Sb}^{5+}$  ions in the available  $4e$  sites. Any suspected differences in the compositions with varying amounts of  $\text{Li}^+$ ,  $\text{Cr}^{3+}$  and  $\text{Sb}^{5+}$  ions were soon disregarded based on the fact that phase pure bulk polycrystalline samples could only be obtained from  $\text{Li}_4\text{CrSbO}_6$  stoichiometry. After several trials, a best match for the observed intensities were obtained for the cationic mixing of (Sb1/Li3), (Li4/Cr1) and (Cr2/Li5/Sb2) to an extent of 0.75/0.25, 0.47/0.53, and 0.45/0.3/0.25 (Fig. 2). In order to obtain a stable least squares refinements,



the thermal and positional parameters were restrained during the verification of the occupancies of the different atoms in the structure. The nominal stoichiometry  $\text{Li}_3(\text{Li}_{1.02}\text{Cr}_{1.00}\text{Sb}_{0.98})\text{O}_6$  was obtained with respective  $R = 4.9\%$ ,  $wR_2 = 11.39\%$  and  $\text{GOF} = 1.255$ . The final crystallographic parameters obtained have been summarized in Tables 1, S7 and S8. A comparison of the intensities obtained from the single crystal measurements, along with the PXRD pattern simulated from the solution, and the PXRD of the bulk sample preparation is shown in Figure S2. Finally, the Reitveld refinement of the PXRD pattern of the bulk samples obtained for  $\text{Li}_4\text{CrSbO}_6$  was carried out. The structural refinement was found to be difficult because of the inherent stacking disorder existing in the structure. Ultimately the refinement converged with small differences in the amount of (Li4/Cr1) and (Cr2/Li5/Sb2) sharing in the two of three  $4e$  sites (Table 1) and with more distorted octahedra. The structure of  $\text{Li}_4\text{CrSbO}_6$  in  $C2/c$  space group could be justified from the PXRD patterns also because of the presence of the predominant amounts of Sb1, Li4 and Cr2 atoms in the three  $4e$  sites forming the Li/Cr/Sb honeycomb octahedral layers (Fig. 2). This is confirmed by the clear appearance of superstructure reflections even in the PXRD data as discussed earlier (Figures 1b and S1 and Table S2). The Li1-O and Li2-O octahedra in the SCXRD solution are almost regular and the bond valences calculated are close to the atomic valence (Table S9). Even for the (Sb1/Li3) $\text{O}_6$  octahedra, the bond valence<sup>29</sup> (4.26) obtained from the bond distances coincided with the value expected from 0.75/0.25 distribution of Sb and Li. Similarly, the bond angles and bond distances calculated for a distribution of 0.45Cr2/0.3Li5/0.25Sb2 from the SXRD solution appeared to be appropriate as shown by the calculated and the bond valence expected from the cationic charges.

The results from PXRD measurements basically differ from the SCXRD solution in the distribution of various cations along with the presence of slightly more distorted octahedra, (Sb1/Li3)O<sub>6</sub>, (Li4/Cr1)O<sub>6</sub>, and (Cr2/Li5/Sb2)O<sub>6</sub> (Fig. 2 and Table S9). These differences might easily be attributed to the relatively lower synthesis temperature (850°C) of the polycrystalline samples as compared to the higher temperature (1100°C) at which the single crystals were obtained as well as to the stacking faults that are invariably present in the polycrystalline samples. The Reitveld refinement of PXRD patterns of Li<sub>4</sub>MnSbO<sub>6</sub> and Li<sub>4</sub>GaSbO<sub>6</sub> (Fig. 1) were also found to be similar to the powder refinement of Li<sub>4</sub>CrSbO<sub>6</sub> (Tables 2 and 3), but with differences again in the distribution of the cations in the various *4e* sites. The structure solution in these oxides strongly confirmed the fact that the ions prefer to reach an almost short of a perfectly ordered structure consisting of regular (SbO<sub>6</sub>), (LiO<sub>6</sub>) and (MO<sub>6</sub>) (M = Mn, Ga) octahedra. Out of the various members of Li<sub>4</sub>MSbO<sub>6</sub> (M = Cr, Mn, Ga) oxides, the Ga analogue possessed much more regular octahedra (Fig. 2) and the corresponding bond valence calculations agreed well (Table S9). The respective PXRD patterns of Li<sub>4</sub>MnSbO<sub>6</sub> and Li<sub>4</sub>GaSbO<sub>6</sub> showed relatively more and less stacking disorders respectively in the 15° > 2θ > 25° region (Fig. 1) and might be the reason for the better structural solution in the Ga based oxide. Our attempts to carry out the Reitveld refinement of isostructural Li<sub>4</sub>AlSbO<sub>6</sub> (*a* = 5.038(9); *b* = 8.7106(7); *c* = 9.727(1) Å; β = 99.7(3)°) was not completely successful because of the additional Li<sub>3</sub>SbO<sub>4</sub> impurity together with higher amount of disorder observed in this sample. Variations in synthetic conditions are being investigated in order to form phase pure Li<sub>4</sub>AlSbO<sub>6</sub> without any impurity. Additionally, the honeycomb layer in Li<sub>4</sub>MnSbO<sub>6</sub> (Fig. 2) revealed the tetragonal compression (reduction in the *b* parameter

(Table 2)) for the  $(\text{Li}_4/\text{Mn}_1)\text{O}_6$  and  $(\text{Mn}_2/\text{Li}_5/\text{Sb}_2)\text{O}_6$  octahedra, as expected for a Jahn-Teller distorted  $\text{Mn}^{3+}(d^3)$  ions.

The most interesting fact in these structures is the preferred cationic mixing resulting in an ordered structure in spite of possessing similar ionic radii specially between  $\text{Sb}^{5+}(\text{VI}) = 0.60\text{\AA}$ , and that of the  $\text{M}^{3+}$  ions ( $\text{Cr}^{3+}(\text{VI}) = 0.615\text{\AA}$ ;  $\text{Mn}^{3+}(\text{VI}) = 0.645\text{\AA}$ ;  $\text{Ga}^{3+}(\text{VI}) = 0.62\text{\AA}$ ). The driving force must be the presence of slightly bigger  $\text{Li}^+$  ions and furthermore mainly to reduce the various cation-cation repulsions possible in these edge shared octahedral structures. Although both in  $\text{Li}_4\text{FeSbO}_6$ , (S.G.  $C2/m$ )<sup>20</sup> and  $\text{Na}_3\text{LiFeSbO}_6$  (S. G.  $C2/c$ )<sup>28</sup> ordering has been expected in the individual  $(\text{LiFeSbO}_6)^{3-}$  layer in order to minimize the cationic interactions of  $\text{Sb}^{5+}\text{-Sb}^{5+}$ ,  $\text{Fe}^{3+}\text{-Fe}^{3+}$  and  $\text{Sb}^{5+}\text{-Fe}^{3+}$  pairs, for the first time the structural solutions have been arrived in the present investigation thereby confirming the cation distribution in these  $\text{Li}_4\text{MSbO}_6$  ( $\text{M} = \text{Cr}, \text{Mn}, \text{Ga}$ ) oxides.

### 3.2 Optical properties

UV-visible diffuse reflectance spectra (Fig. S3(a)) of  $\text{Li}_4\text{MSbO}_6$  ( $\text{M} = \text{Cr}, \text{Mn}, \text{Fe}, \text{Al}, \text{Ga}$ ) oxides showed clearly the distinction in the color of these oxides (green for Cr and brick red for Mn), to that of Al and Ga (white). Examination of the spectra showed only the absorption edge around 300nm in the UV region for the white colored  $\text{Li}_4\text{AlSbO}_6$  and  $\text{Li}_4\text{GaSbO}_6$  oxides. For the rest of the transition metal ( $\text{M}(\text{III}) = \text{Cr}, \text{Mn}, \text{Fe}$ ) containing oxides, in addition to the absorption edges in the visible regions, the absorptions due to the  $d\text{-}d$  electronic transitions are also observed. As shown earlier,<sup>30</sup> in the series  $\text{Na}_3\text{Ni}_{2-x}\text{Cu}_x\text{SbO}_6$  ( $x = 0, 0.5, 1, 1.5, 2$ ) and  $\text{Na}_3\text{Cu}_{2-x}\text{M}_x\text{SbO}_6$  ( $\text{M} = \text{Mg}$  or  $\text{Zn}$  and  $0 \leq x \leq 1.5$ ) it might be feasible to have intermediate solid solution members involving the various

M(III) = Fe, Al, Ga ions in order to tune the band gaps. Furthermore, PL spectra with  $\lambda = 560$  nm and 360 nm were also recorded for  $\text{Li}_4\text{CrSbO}_6$  and  $\text{Li}_4\text{MnSbO}_6$  respectively (Fig. S3(b)). Strong emission bands observed at 708 nm ( ${}^2\text{E}(t_2^3) \rightarrow {}^4\text{A}_2(t_2^3)$ ) characteristic for the presence of  $\text{Cr}^{3+}$  ions<sup>30</sup> are observed. For  $\text{Mn}^{3+}$  emission bands were observed at 415 nm and 440 nm.

### 3.3 Ion-Exchange behaviour and Ionic Conductivity

$\text{Li}_4\text{MSbO}_6$  oxides with interlayer lithium ions (Fig. S4) found to undergo facile ion-exchange reactions with  $\text{AgNO}_3$  leading to delafossite-type oxides as noted before. The ion-exchange reactions result in layer gliding and the ordered rocksalt structures often end up in delafossite-type phases with the ordering intact resulting in superstructures.<sup>14, 32</sup> In the present case, the PXRD patterns (Fig. S5) confirmed the formation of ordered delafossites and the refined cell parameters ( $a \approx 5.3\text{\AA}$ ;  $c \approx 18.7\text{\AA}$ ) using Le Bail fitting procedure in S.G.  $P3_1I2$  are listed in Table S10. The silver delafossite oxides are found to be stable up to temperatures of 1000 K as indicated by their thermogravimetric measurements obtained by measuring the weight loss on heating these oxides in air. The introduction of  $\text{Ag}^+$  ions directly influences the electronic structure of the oxides in such a way that the absorption edges are shifted towards more in the visible region (Fig. S6) and are very clearly observed in the  $\text{Ag}_3\text{LiAlSbO}_6$  and  $\text{Ag}_3\text{LiGaSbO}_6$  oxides as compared to their parent lithium analogues (Fig. S3a).

The ion-exchange behaviour of these oxides indicated a good ionic mobility and conductivities of  $\text{Li}_4\text{MSbO}_6$  (M = Cr, Fe, Al) were measured. The conductivity values at 573K and the activation energies (Cr:  $4.31 \times 10^{-6}$  S  $\text{cm}^{-1}$ , 0.66 eV; Fe:  $3.66 \times 10^{-6}$  S  $\text{cm}^{-1}$ , 0.57 eV; Mn:  $9.33 \times 10^{-5}$ , 0.57eV; Al:  $3.05 \times 10^{-6}$  S  $\text{cm}^{-1}$ , 0.91 eV) are found to be nominal

(Fig. 3). While the electronic conductivities of these oxides are expected to be negligible as compared to their ionic conductivities in the temperature range of 300-573K, the electronic conductivities may sufficiently increase at higher temperatures specially for oxides such as  $\text{Li}_4\text{CrSbO}_6$  and  $\text{Li}_4\text{MnSbO}_6$ .

### 3.4 Magnetic Measurements

The plots showing the variation of the magnetic susceptibilities of  $\text{Li}_4\text{CrSbO}_6$  and  $\text{Li}_4\text{MnSbO}_6$  with temperature are shown in Fig. 4. A Curie-Weiss behavior in the temperature range 300K - 75K resulted in a magnetic moment of  $4.5\mu\text{B}$  for  $\text{Li}_4\text{CrSbO}_6$ . The calculated value of  $3.87\mu\text{B}$  by taking  $\text{Cr}^{3+}$  (high spin  $3d^3$ ) agreed with the observed value. A negative Weiss constant ( $\Theta = -67\text{K}$ ) together with a curved signature at very low temperature (7K) indicated the presence of antiferromagnetic interactions. In the case of  $\text{Li}_4\text{MnSbO}_6$ , the Curie-Weiss behavior was observed in the temperature range 300 - 50K and the experimentally observed magnetic moments has been found to be  $4.49\mu\text{B}$  corresponding to the calculated value of  $4.89\mu\text{B}$  for  $\text{Mn}^{3+}$  ( $3d^4$ ) ions. Here again a negative weiss constant ( $-68\text{K}$ ) confirmed the possibility of antiferromagnetic interactions. Correspondingly, a dip in the plot of inverse magnetic susceptibility with temperature is noted. The behavior of divalent ions (Co, Ni, Cu) and that of trivalent  $\text{Fe}^{3+}$  ions forming the honeycomb lattices result in complex magnetic properties and have been investigated. For example in  $\text{Li}_4\text{FeSbO}_6$ , the honeycomb lattices with lesser amount of the trivalent ions (as compared to, for example  $\alpha\text{-NaFeO}_2$ ) have been characterized in detail.<sup>20</sup> The onset of antiferromagnetic order has been shown at 3.6 K along with a Curie-Weiss behavior and a negative Weiss ( $\Theta$ ) value of  $-17\text{K}$ . In the case of  $\text{Na}_3\text{Co}_2\text{SbO}_6$ , and  $\text{Na}_2\text{Co}_2\text{TeO}_6$  with  $\text{Co}^{2+}$  ions in high spin configuration, the magnetic

susceptibility data revealed ferromagnetic and antiferromagnetic interactions.<sup>13, 33</sup>  $\text{Li}_3\text{Ni}_2\text{SbO}_6$  and  $\text{Na}_3\text{Ni}_2\text{SbO}_6$  exhibited similar antiferromagnetic order at low temperatures (15K, 18K respectively).<sup>15, 30</sup> Significant Spin-gap behavior has been observed in  $\text{Na}_3\text{Cu}_2\text{SbO}_6$  and  $\text{Na}_2\text{Cu}_2\text{TeO}_6$  oxides<sup>30, 5</sup> and Jahn-Teller distortion of  $\text{Cu}^{2+}$  ions in these oxides were cited to be responsible.

#### 4. Conclusions

$\text{Li}_4\text{MSbO}_6$  (M(III) = Cr, Mn, Al, Ga) oxides are found to be of the rock salt type with clear evidence of additional ordering resulting in superstructure (S.G.  $C2/c$ ) from the preferred mixing of cations in the honeycomb layers ( $\text{LiMSbO}_6$ )<sup>3-</sup>. Although such an ordering was considered in the earlier investigation involving  $\text{Li}_4\text{FeSbO}_6$  (S.G.  $C2/m$ ), the evidence from the PXRD based structural elucidations was missing. The reported oxides undergo facile ion-exchange reactions and the ionic conductivity measurements confirm the mobility of the interlayer lithium ions. The magnetic susceptibility measurements with varying temperature showed Curie-Weiss behavior in the temperature range of (300-75K) for  $\text{Li}_4\text{CrSbO}_6$  and in the range (300-50K) for  $\text{Li}_4\text{MnSbO}_6$  oxides with negative  $\Theta$  values. The onset of antiferromagnetism is being indicated for  $\text{Li}_4\text{CrSbO}_6$  at 7K, and for  $\text{Li}_4\text{MnSbO}_6$  on the other hand deviated from the Curie-Weiss behavior at low temperatures without the sharp decrease in the  $\chi$  values and did not show a clear signal even at very low temperatures. The introduction of redox type metal ions along with more of lithium ions in these new oxide compositions are indeed promising candidates for the identification and characterization of novel electrode materials for lithium ion batteries.

#### Acknowledgement

This work was supported by the DST (SR/S1/PC-07/2011), DST - Nanomission Government of India, and University of Delhi under the “Scheme to strengthen R & D Doctoral Research Program”. We thank the USIC, DU, for the SXRD facilities. NB and AG thank the CSIR for SRF and DST, Government of India for fellowships respectively.

## References

- [1] M. S. Whittingham, *Mater. Res. Bull.*, 2008, **33**, 411; J. B. Goodenough and Y. Kim, *Chem. Mater.*, 2010, **22**, 587; R. A. Huggins, *Advanced Batteries, Materials Science Aspects*, Springer: New York, 2009.
- [2] J. Molenda, C. Delmas and P. Hagenmuller, *Solid State Ionics*, 1983, **9 – 10**, 431; J. Molenda, C. Delmas, P. Dordor and A. Stokłosa, *Solid State Ionics*, 1989, **12**, 473; M. Lee, L. Viciu, L. Li, Y. Wang, M. L. Foo, S. Watauchi, R. A. Jr. Pascal, R. J. Cava and N. P. Ong, *Nat. Mater.*, 2006, **5**, 537; K. Takada, H. Sakurai, E. Takayama-Muromachi, F. Izumi, R. A. Dilanian and T. Sasaki, *Nature*, 2003, **422**, 53.
- [3] J. J. Braconnier, C. Delmas, C. Fouassier and P. Hagenmuller, *Mater. Res. Bull.*, 1980, **15**, 1797; R. Berthelot, D. Carlier and C. Delmas, *Nat. Mater.*, 2011, **10**, 74; M. Guignard, C. Didier, J. Darriet, P. Bordet, E. Elkaim and C. Delmas, *Nat. Mater.*, 2013, **12**, 74.
- [4] G. Mather, C. Dussarrat, J. Etourneau, and A. R. West, *J. Mater. Chem.*, 2000, **10**, 2219.
- [5] J. Xu, A. Assoud, N. Soheilnia, S. Derakhshan, H. L. Cuthbert, J. E. Greedan, M. H. Whangbo and H. Kleinke, *Inorg. Chem.*, 2005, **44**, 5042.
- [6] M. A. Evstigneeva, V. B. Nalbandyan, A. A. Petrenko, B. S. Medvedev and A. A. Kataev, *Chem. Mater.*, 2011, **23**, 1174.

- [7] R. Berthelot, W. Schmidt, A. W. Sleight and M. A. Subramanian, *J. Solid State Chem.*, 2012, **196**, 225.
- [8] C. Greaves and S. M. A. Katib, *Mater. Res. Bull.*, 1990, **25**, 1175.
- [9] G. C. Mather, R. I. Smith, J. M. S. Skakle, J. G. Fletcher, M. A. Castellanos, M. P. Gutierrez and A. R. West, *J. Mater. Chem.*, 1995, **5**, 1177.
- [10] G. C. Mather and A. R. West, *J. Solid State Chem.*, 1996, **124**, 214.
- [11] J. M. S. Skakle, R. M. A. Castellanos, S. T. Tovar and A. R. West, *J. Solid state Chem.*, 1997, **131**, 115.
- [12] O. A. Smirnova, V. B. Nalbandyan, A. A. Petrenko and M. Avdeev, *J. Solid State Chem.*, 2005, **178**, 1165.
- [13] L. Viciu, Q. Huang, E. Morosan, H. W. Zandbergen, N. I. Greenbaum, T. McQueen and R. J. Cava, *J. Solid State Chem.*, 2007, **180**, 1060.
- [14] V. V. Politaev, V. B. Nalbandyan, A. A. Petrenko, I. L. Shukaev, V. A. Volotchaev and B. S. Medvedev, *J. Solid State Chem.*, 2010, **183**, 684.
- [15] E. A. Zvereva, M. A. Evstigneeva, V. B. Nalbandyan, O. A. Savelieva, S. A. Ibragimov, O. S. Volkova, L. I. Medvedeva, A. N. Vasiliev, R. Klingeler and B. Buechner, *Dalton Trans.*, 2012, **41**, 572.
- [16] R. Berthelot, W. Schmidt, S. Muir, J. Eilertsen, L. Etienne, A. W. Sleight and M. A. Subramanian, *Inorg. Chem.*, 2012, **51**, 5377; E. M. Seibel, J. H. Roudebush, H. Wu, Q. Huang, M. N. Ali, H. Ji and R. J. Cava, *Inorg. Chem.*, 2013, **52**, 13605.
- [17] V. Kumar, N. Bhardwaj, N. Tomar, V. Thakral and S. Uma, *Inorg. Chem.*, 2012, **51**, 10471.
- [18] V. Kumar, A. Gupta and S. Uma, *Dalton Trans.*, 2013, **42**, 14992.



- [19] V. B. Nalbandyan, M. Avdeev, M. A. Evstigneeva, *J. Solid State Chem.*, 2013, **199** 62.
- [20] E. A. Zvereva, O. A. Savelieva, D. Ya. Titov, M. A. Evstigneeva, V. B. Nalbandyan, C. N. Kao, J.-Y. Lin, I. A. Presniakov, A. V. Sobolev, S. A. Ibragimov, M. Abdel-Hafiez, Yu. Krupskaya, C. Jähne, G. Tan, R. Klingeler, B. Büchnerb and A. N.Vasilieva, *Dalton Trans.*, 2013, **42**, 1550.
- [21] M. Sathiya, K. Ramesha, G. Rouse, D. Foix, D. Gonbeau, K. Guruprakash, A. S. Prakash, A. S. Doublete and J.-M. Tarascon, *Chem Comm.*, 2013, **49**, 11376.
- [22] A. C. Larson and R. B. VonDreele, General Structure Analysis System (GSAS), Los Alamos National Laboratory Report LAUR 2004, 86-748; B. H. Toby, *J. Appl. Cryst.*, 2001, **34**, 210.
- [23] G. M. Sheldrick, SHELXL97, Program for crystal structure refinement; University of Gottingen: Germany, 1997.
- [24] L. Farrugia, *J. Appl. Crystallogr.*, 1999, **32**, 837.
- [25] A. Riou, A. Lecerf, Y. Gerault and Y. Cudenneq, *Mater. Res. Bull.*, 1992, **27**, 269.
- [26] J. F. Dorrian and R. E. Newnham, *Mater. Res. Bull.* 1969, **4**, 179.
- [27] S. Laha, E. Morán, R. Sáez-Puche, M. Á. Alario-Franco, A. J. Dossantos-Garcia, E. Gonzalo, A. Kuhn, F. García-Alvarado, T. Sivakumar, S. Tamilarasan, S. Natarajan and J. Gopalakrishnan, *J. Solid State Chem.*, 2013, **203**, 160.
- [28] W. Schmidt, R. Berthelot, L. Etienne, A. Wattiaux and M. A. Subramanian, *Mater. Res. Bull.*, 2014, **50**, 292.

- [29] I. D. Brown, *The Chemical Bond in Inorganic Chemistry: The Bond Valence Model*; Oxford University Press: Oxford, 2002; I. D. Brown, *Chem. Rev.*, 2009, **109**, 6858; I. D. Brown, *Z. Kristallogr.*, 1992, **199**, 255.
- [30] W. Schmidt, R. Berthelot, A. W. Sleight and M. A. Subramanian, *J. Solid State Chem.*, 2013, **201**, 178.
- [31] W. M. Yen, S. Shionoya and H. Yamamoto, *Phosphor Handbook*, Taylor and Francis, Second edition, 2006.
- [32] R. Nagarajan, S. Uma, M. K. Jayaraj, J. Tate, and A. W. Sleight, *Solid State Sci.*, 2002, **4**, 787.
- [33] E. M. Seibel, J. H. Roudebush, H. Wu, Q. Huang, M. N. Ali, H. Ji and R. J. Cava, *Inorg. Chem.*, 2013, **52**, 13605.

### List of Tables and Figures

**Table 1:** Positional parameters, occupancies and thermal parameters of  $\text{Li}_4\text{CrSbO}_6$  from SXRD (bold) and PXRD measurements.

**Table 2:** Crystallographic (PXRD) parameters of  $\text{Li}_4\text{MSbO}_6$  (M = Cr, Mn, Ga).

**Table 3:** Positional, occupancies and thermal parameters for  $\text{Li}_4\text{MSbO}_6$  (M = Mn, Ga).

**Fig. 1** PXRD patterns of (a)  $\text{Li}_4\text{FeSbO}_6$ , (b)  $\text{Li}_4\text{CrSbO}_6$ , (c)  $\text{Li}_4\text{MnSbO}_6$ , (d)  $\text{Li}_4\text{AlSbO}_6$ , (e)  $\text{Li}_4\text{GaSbO}_6$  ((b-e) red, experimental data; green line, calculated profile; pink line below, difference profile; vertical bars, Bragg positions. (The inset in b-e shows the region  $20^\circ < 2\theta < 40^\circ$  wherein the additional reflections attributed to  $C2/c$  are marked with arrows; asterisk refers to  $\text{Li}_3\text{SbO}_4$  impurity.)

**Fig. 2** Representation of Honeycomb type structure of  $\text{Li}_3\text{LiMSbO}_6$  series for M = (a) Cr (SXRD solution), (b) Cr (PXRD solution), (c) Mn, (d) Ga.

**Fig. 3** Ionic Conductivity plots of  $\text{Li}_4\text{MSbO}_6$  for M = Cr, Mn, Fe and Al.

**Fig. 4** The temperature dependence of magnetic susceptibility plots at H=1T for (a)  $\text{Li}_4\text{CrSbO}_6$  and (b)  $\text{Li}_4\text{MnSbO}_6$ . The insets show the respective plots of inverse susceptibility with temperature.

**Table 1:** Positional parameters, occupancies and thermal parameters of  $\text{Li}_4\text{CrSbO}_6$  from SXR D (bold) and PXR D measurements.

Atom	Site	S.O.F	<i>x</i>	<i>y</i>	<i>z</i>	$U_{iso}$
Li1	<i>8f</i>	1	0.244	0.07682	0.004	0.025
<b>Li1</b>	<b><i>8f</i></b>	<b>1</b>	<b>0.245(2)</b>	<b>0.0785(13)</b>	<b>0.0004(10)</b>	<b>0.020(3)</b>
Li2	<i>4d</i>	1	0.25	0.25	0.5	0.025
<b>Li2</b>	<b><i>4d</i></b>	<b>1</b>	<b>0.25</b>	<b>0.25</b>	<b>0.5</b>	<b>0.023(4)</b>
Sb1/Li3	<i>4e</i>	0.76/0.24	0	0.7478(4)	0.25	0.025
<b>Sb1/Li3</b>	<b><i>4e</i></b>	<b>0.75/0.25</b>	<b>0</b>	<b>0.75128(7)</b>	<b>0.25</b>	<b>0.0061(3)</b>
Li4/Cr1	<i>4e</i>	0.61/0.39	0	0.0889(10)	0.25	0.025
<b>Li4/Cr1</b>	<b><i>4e</i></b>	<b>0.47/0.53</b>	<b>0</b>	<b>0.0869(4)</b>	<b>0.25</b>	<b>0.0254(8)</b>
Cr2/Li5/Sb2	<i>4e</i>	0.61/0.17/0.22	0	0.41418	0.25	0.025
<b>Cr2/Li5/Sb2</b>	<b><i>4e</i></b>	<b>0.45/0.3/0.25</b>	<b>0</b>	<b>0.4194(1)</b>	<b>0.25</b>	<b>0.0029(4)</b>
O1	<i>8f</i>	1	0.1300(16)	0.2793(13)	0.1176(10)	0.025
<b>O1</b>	<b><i>8f</i></b>	<b>1</b>	<b>0.1380(10)</b>	<b>0.2546(5)</b>	<b>0.1363(5)</b>	<b>0.0137(11)</b>
O2	<i>8f</i>	1	0.1072(18)	0.5987(5)	0.1401(10)	0.025
<b>O2</b>	<b><i>8f</i></b>	<b>1</b>	<b>0.1175(10)</b>	<b>0.5876(5)</b>	<b>0.1360(5)</b>	<b>0.0129(11)</b>
O3	<i>8f</i>	1	0.1162(21)	0.8892(11)	0.1336(10)	0.025
<b>O3</b>	<b><i>8f</i></b>	<b>1</b>	<b>0.1288(10)</b>	<b>0.9106(5)</b>	<b>0.1347(5)</b>	<b>0.0139(11)</b>

**Table 2:** Crystallographic (PXRD) parameters of  $\text{Li}_4\text{MSbO}_6$  (M = Cr, Mn, Ga).

	$\text{Li}_4\text{CrSbO}_6$	$\text{Li}_4\text{MnSbO}_6$	$\text{Li}_4\text{GaSbO}_6$
<b>Crystal system</b>	Monoclinic	Monoclinic	Monoclinic
<b>Space group</b>	<i>C 1 2/c 1</i>	<i>C 1 2/c 1</i>	<i>C 1 2/c 1</i>
<b>Lattice constants:</b>			
<i>a</i> (Å)	5.1238(1)	5.0965(6)	5.13076(7)
<i>b</i> (Å)	8.8449(1)	8.8270(2)	8.8794(1)
<i>c</i> (Å)	9.7982(2)	9.8542(1)	9.8607(1)
$\beta$ (°)	100.011(2)	99.9119(7)	100.023(1)
<b>Cell volume</b> (Å <sup>3</sup> )	437.29(1)	436.69(1)	442.385(6)
<b>Formula weight</b>	295.2	294.63	314.37
<b>Z</b>	8	8	8
<b>Density (calc.)</b>	4.48 g cm <sup>-3</sup>	4.48 g cm <sup>-3</sup>	4.72 g cm <sup>-3</sup>
<b>Radiation</b>	CuK $\alpha$	CuK $\alpha$	CuK $\alpha$
<b>2<math>\theta</math> range</b>	10 - 70°	10 - 70°	10 - 70°
<b>No. of data points</b>	4570	4199	4570
<b>No. of reflections</b>	96	93	98
<b>No. of parameters</b>	28	31	22
<b>Agreement factors:</b>			
<b>R<sub>p</sub></b>	6.58%	2.68%	6.07%
<b>R<sub>wp</sub></b>	8.70%	3.56 %	8.49%
<b><math>\chi^2</math></b>	8.72	17.85	8.510

**Table 3:** Positional, occupancies and thermal parameters for  $\text{Li}_4\text{MSbO}_6$  (M = Mn, Ga).

<b><math>\text{Li}_4\text{MnSbO}_6</math></b>					
<b>Atom</b>	<b>Site</b>	<b>S.O.F</b>	<b>x</b>	<b>y</b>	<b>z</b>
<b>Li1</b>	<i>8f</i>	1	0.3147(14)	0.0408(11)	-0.0035(8)
<b>Li2</b>	<i>4d</i>	1	0.25	0.25	0.5
<b>Sb1/Li3</b>	<i>4e</i>	0.866(2)/0.134(2)	0	0.75099(7)	0.25
<b>Li4/Mn1</b>	<i>4e</i>	0.837(4)/0.163(4)	0	0.0647(6)	0.25
<b>Mn2/Li5/Sb2</b>	<i>4e</i>	0.917/0.033/0.05	0	0.41828	0.25
<b>O1</b>	<i>8f</i>	1	0.1938(5)	0.2751(5)	0.1366(4)
<b>O2</b>	<i>8f</i>	1	0.1409(4)	0.5937(4)	0.1378(5)
<b>O3</b>	<i>8f</i>	1	0.1304(4)	0.9202(4)	0.1188(6)
<b><math>\text{Li}_4\text{GaSbO}_6</math></b>					
<b>Li1</b>	<i>8f</i>	1	0.29026	0.09414	-0.00847
<b>Li2</b>	<i>4d</i>	1	0.25	0.25	0.5
<b>Sb1/Li3</b>	<i>4e</i>	0.94/0.058	0	0.7519(2)	0.25
<b>Li4/Ga1</b>	<i>4e</i>	0.87/0.13	0	0.0918(18)	0.25
<b>Ga2/Li5/Sb2</b>	<i>4e</i>	0.87/0.08/0.05	0	0.4194	0.25
<b>O1</b>	<i>8f</i>	1	0.1668(16)	0.2625(14)	0.1447(7)
<b>O2</b>	<i>8f</i>	1	0.1478(18)	0.5927(15)	0.1171(8)
<b>O3</b>	<i>8f</i>	1	0.1465(18)	0.9055(15)	0.1346(7)

(Uiso\* fixed at a constant value of 0.025)

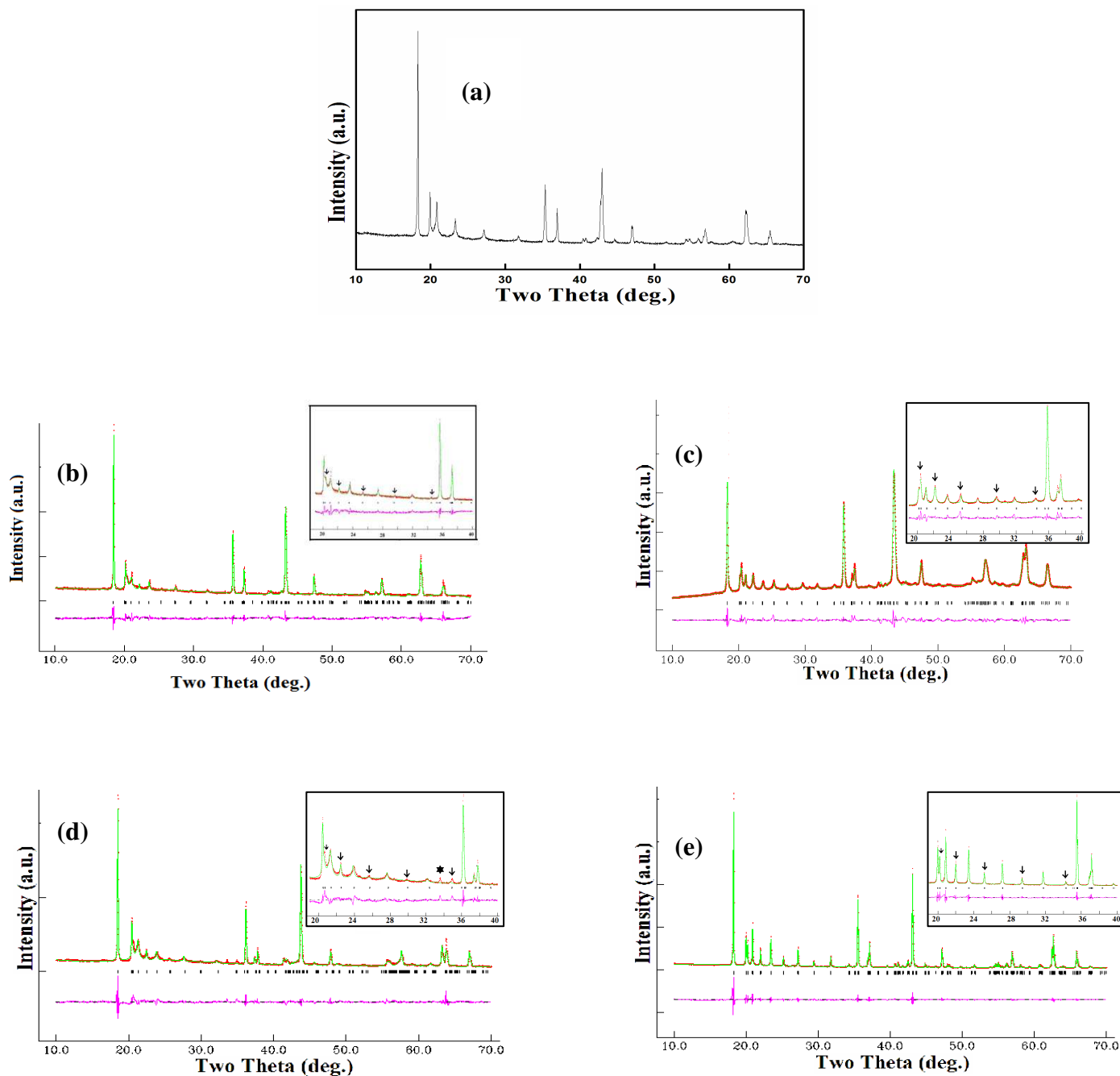


**Fig. 1** PXRD patterns of (a)  $\text{Li}_4\text{FeSbO}_6$ , (b)  $\text{Li}_4\text{CrSbO}_6$ , (c)  $\text{Li}_4\text{MnSbO}_6$ , (d)  $\text{Li}_4\text{AlSbO}_6$ , (e)  $\text{Li}_4\text{GaSbO}_6$  ((b-e) red, experimental data; green line, calculated profile; pink line below, difference profile; vertical bars, Bragg positions. (The inset in b-e shows the region  $20^\circ < 2\theta < 40^\circ$  wherein the additional reflections attributed to  $C2/c$  are marked with arrows; asterisk refers to  $\text{Li}_3\text{SbO}_4$  impurity.)

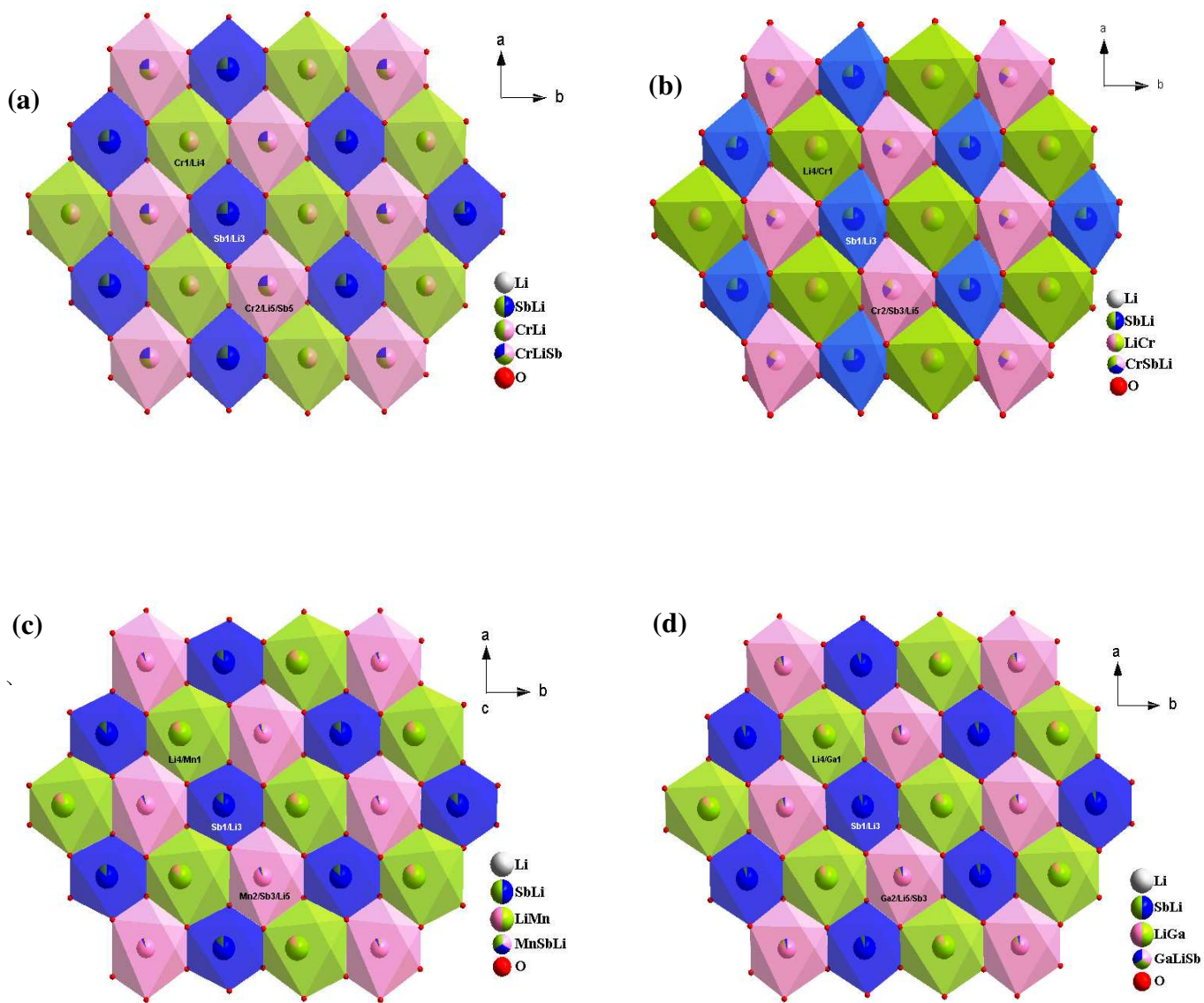


**Fig. 2** Representation of Honeycomb type structure of  $\text{Li}_3\text{LiMSbO}_6$  series for  $M =$  (a) Cr (SXR solution), (b) Cr (PXR solution), (c) Mn, (d) Ga.



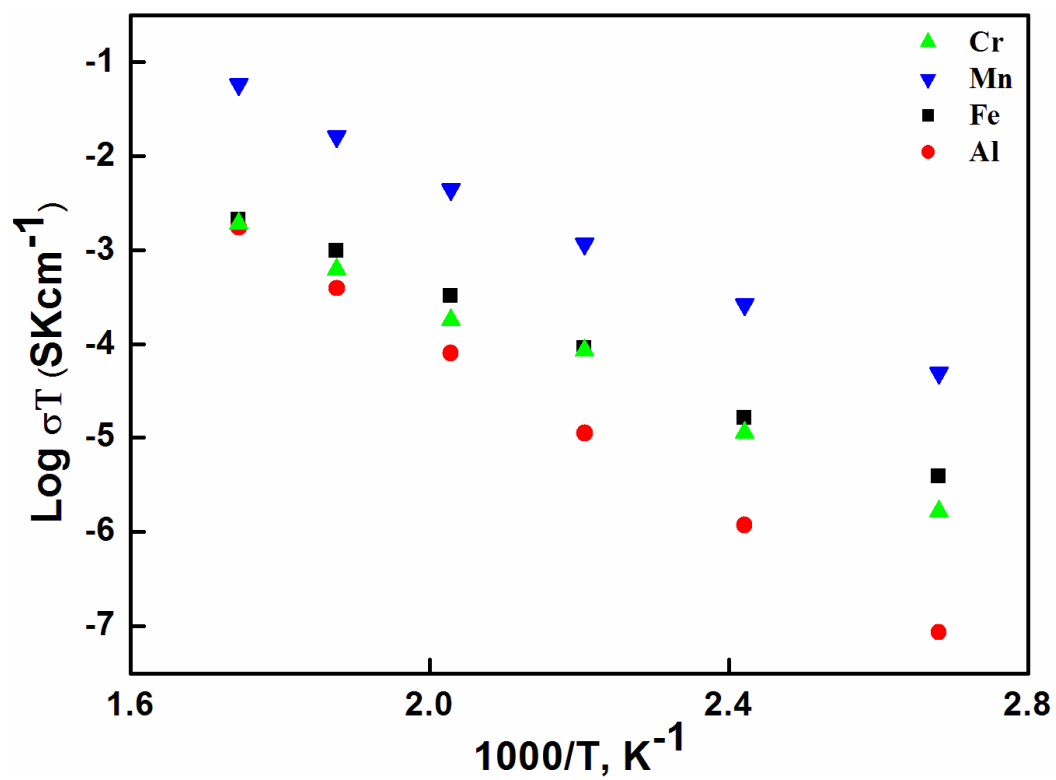


**Fig. 3** Ionic Conductivity plots of  $\text{Li}_4\text{MSbO}_6$  for  $M = \text{Cr, Mn, Fe}$  and  $\text{Al}$ .

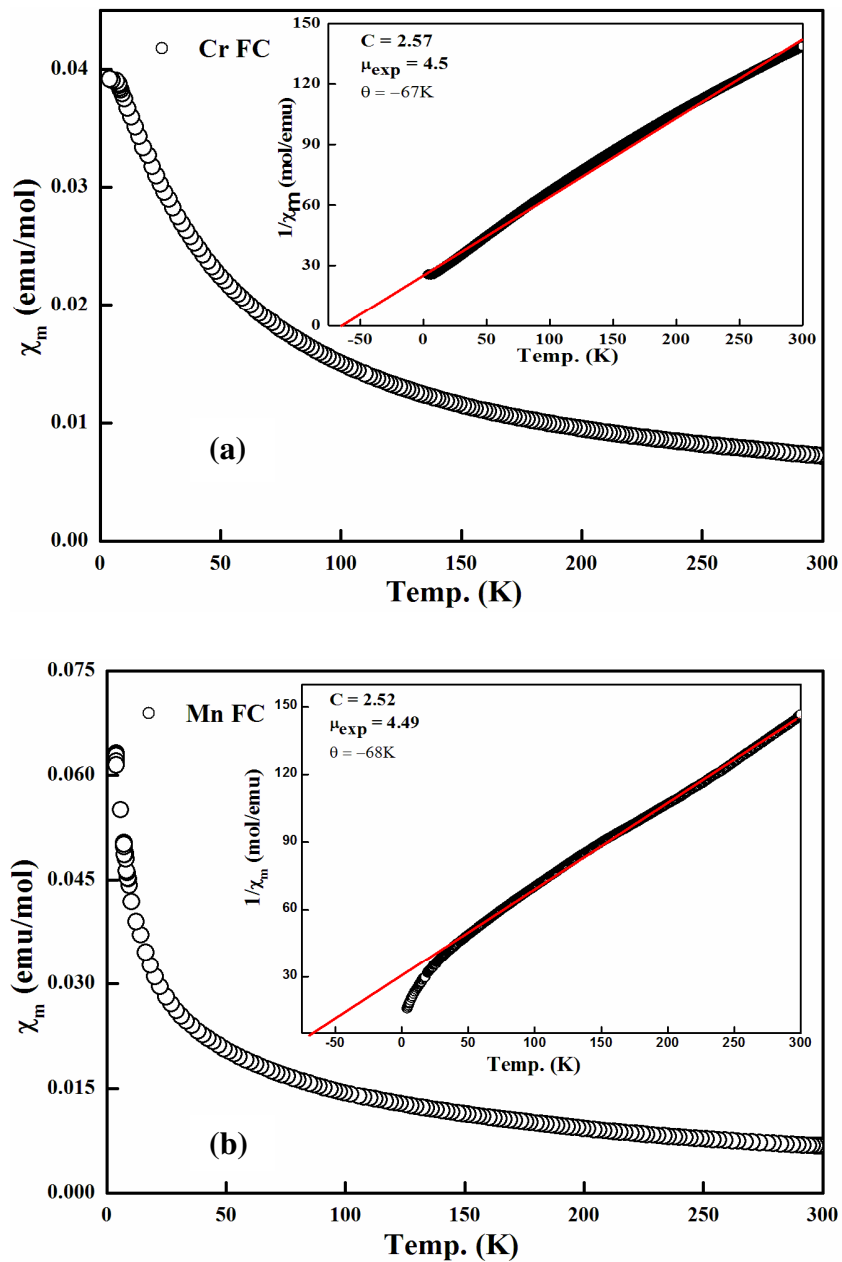


**Fig. 4** The temperature dependence of magnetic susceptibility plots at  $H = 1\text{ T}$  for (a)  $\text{Li}_4\text{CrSbO}_6$  and (b)  $\text{Li}_4\text{MnSbO}_6$ . The insets show the respective plots of inverse susceptibility with temperature.

# Evidence of Cationic Mixing and Ordering in the Honeycomb Layer of $\text{Li}_4\text{MSbO}_6$ (M(III) = Cr, Mn, Al, Ga) (S.G. $C2/c$ ) Oxides

Neha Bhardwaj, Akanksha Gupta and S. Uma\*

Materials Chemistry Group, Department of Chemistry,

University of Delhi, Delhi 110 007, INDIA

## Table of contents Graphic

